

## Research Article

# A $\text{CaMoO}_4$ Crystal Low Temperature Detector for the AMoRE Neutrinoless Double Beta Decay Search

G. B. Kim,<sup>1,2,3</sup> S. Choi,<sup>2</sup> F. A. Danevich,<sup>4</sup> A. Fleischmann,<sup>5</sup> C. S. Kang,<sup>1,3</sup>  
H. J. Kim,<sup>6</sup> S. R. Kim,<sup>1,3</sup> Y. D. Kim,<sup>1,7</sup> Y. H. Kim,<sup>1,3,8</sup> V. A. Kornoukhov,<sup>9</sup> H. J. Lee,<sup>1,3</sup>  
J. H. Lee,<sup>3</sup> M. K. Lee,<sup>3</sup> S. J. Lee,<sup>3,10</sup> J. H. So,<sup>1,3</sup> and W. S. Yoon<sup>1,3,8</sup>

<sup>1</sup> Institute for Basic Science, Daejeon 305-811, Republic of Korea

<sup>2</sup> Department of Physics and Astronomy, Seoul National University, Seoul 151-747, Republic of Korea

<sup>3</sup> Korea Research Institute of Standards and Science, Daejeon 305-340, Republic of Korea

<sup>4</sup> Institute for Nuclear Research, 03680 Kyiv, Ukraine

<sup>5</sup> Kirchhoff-Institut für Physik, Universität Heidelberg, 69120 Heidelberg, Germany

<sup>6</sup> Physics Department, Kyungpook National University, Daegu 702-701, Republic of Korea

<sup>7</sup> Department of Physics, Sejong University, Seoul 143-747, Republic of Korea

<sup>8</sup> Korea University of Science and Technology, Daejeon 305-350, Republic of Korea

<sup>9</sup> Institute for Theoretical and Experimental Physics, 117218 Moscow, Russia

<sup>10</sup> NASA Goddard Space Flight Center, Greenbelt, MD 20771, USA

Correspondence should be addressed to Y. H. Kim; [yhk@ibs.re.kr](mailto:yhk@ibs.re.kr)

Received 4 July 2014; Accepted 30 August 2014

Academic Editor: Hiro Ejiri

Copyright © 2015 G. B. Kim et al. This is an open access article distributed under the Creative Commons Attribution License, which permits unrestricted use, distribution, and reproduction in any medium, provided the original work is properly cited. The publication of this article was funded by SCOAP<sup>3</sup>.

We report the development of a  $\text{CaMoO}_4$  crystal low temperature detector for the AMoRE neutrinoless double beta decay ( $0\nu\beta\beta$ ) search experiment. The prototype detector cell was composed of a 216 g  $\text{CaMoO}_4$  crystal and a metallic magnetic calorimeter. An overground measurement demonstrated FWHM resolution of 6–11 keV for full absorption gamma peaks. Pulse shape discrimination was clearly demonstrated in the phonon signals, and  $7.6\sigma$  of discrimination power was found for the  $\alpha$  and  $\beta/\gamma$  separation. The phonon signals showed rise-times of about 1 ms. It is expected that the relatively fast rise-time will increase the rejection efficiency of two-neutrino double beta decay pile-up events which can be one of the major background sources in  $0\nu\beta\beta$  searches.

## 1. Introduction

Recent neutrino oscillation experiments have been unveiling the properties of neutrinos [1, 2]. Their experimental evidences strongly suggest that neutrinos are massive and encounter flavor mixing of mass eigenvalues. The mixing angles and the differences between the square masses have been estimated. However, those observations do not provide a direct measurement of the absolute mass and do not answer the question of whether neutrino is its own antiparticle (Majorana-type) or not (Dirac-type).

Search for neutrinoless double beta decay ( $0\nu\beta\beta$ ) is a key experiment to reveal unanswered nature of neutrinos [3–7]. The double beta decay ( $2\nu\beta\beta$ ) that accompanies the simultaneous emission of two electrons and two antineutrinos is a rare process that is an allowed transition in the standard model. Another type of double beta decay that does not emit any neutrinos,  $0\nu\beta\beta$ , can occur if neutrino is massive Majorana particles (i.e., it is its own antiparticle). In the  $0\nu\beta\beta$  process, the full available energy of the decay is carried by the two electrons and the recoiled daughter which has a very small amount of energy compared with that of the electrons.

Therefore, while the electron sum energy spectrum in the  $2\nu\beta\beta$  is continuous up to the available energy release ( $Q_{\beta\beta}$ ), in the  $0\nu\beta\beta$ , the spectrum should have a sharp peak at  $Q_{\beta\beta}$  [2].

The observation of  $0\nu\beta\beta$  would clearly demonstrate that neutrino is not Dirac-type but rather is Majorana-type particle. In that case, physical processes that do not conserve lepton number would be allowed. Moreover, the absolute mass scale, so-called ‘‘effective Majorana neutrino mass’’,  $\langle m_\nu \rangle$ , can be estimated using the  $0\nu\beta\beta$  half life ( $T_{1/2}^{0\nu}$ ),

$$(T_{1/2}^{0\nu})^{-1} = G^{0\nu} |M^{0\nu}|^2 \frac{\langle m_\nu \rangle^2}{m_e^2}, \quad (1)$$

where  $m_e$  is the electron mass,  $G^{0\nu}$  is the kinematic phase-space factor calculable with reasonable precision, and  $M^{0\nu}$  is the model dependent nuclear matrix element. Here, the Majorana mass is defined as

$$\langle m_\nu \rangle = \left| \sum U_{ej}^2 m_j \right|, \quad (2)$$

where the  $m_j$ 's are the mass eigenstates of the neutrino and  $U_{ej}$ 's are the elements of the mixing matrix between the flavor states and mass eigenstates.

Experimentally, the measurement limit of half life is often used as the sensitivity to probe the rare event [7]. In a measurement with nonnegligible backgrounds, the sensitivity becomes

$$T_{1/2}^{0\nu} \propto \delta \varepsilon \sqrt{\frac{Mt}{b\Delta E}}, \quad (3)$$

where  $\delta$  is the concentration of  $\beta\beta$  isotope in the detector,  $\varepsilon$  is the detection efficiency,  $M$  is the detector mass,  $t$  is the measurement time,  $b$  is the background rate per unit mass and energy, and  $\Delta E$  is the energy resolution of the detector, in other words, the region of interest (ROI) of the energy window at the  $Q_{\beta\beta}$  value. However, in a case of a zero-background experiment that observes no event in ROI during the measurement time, the sensitivity becomes proportional to the detector mass and the measurement time,

$$T_{1/2}^{0\nu} \propto \delta \varepsilon Mt. \quad (4)$$

To increase the detection sensitivity, it is essential to have a detector with high concentration of the isotope of interest, detection efficiency, energy resolution, and efficient background rejection capability as well as to minimize backgrounds from internal and external sources in the region of interest. High energy resolution and detection efficiency experiment can be realized with crystal detectors containing the isotope of interest. The detector performance of recently developed low temperature detectors (LTDs) that operate at sub-Kelvin temperatures can perfectly meet the requirements by utilizing state-of-the-art detector technologies with extreme energy sensitivity, such as neutron transmutation doped (NTD) Ge thermistors, superconducting transition edge sensors (TESs), or metallic magnetic calorimeters (MMCs) [8].

The AMoRE (Advanced Mo-based Rare process Experiment) project is an experiment to search for  $0\nu\beta\beta$  of  $^{100}\text{Mo}$  [9]. AMoRE uses  $\text{CaMoO}_4$  crystals as the absorber and MMCs as the sensor [10, 11].  $\text{CaMoO}_4$  is a scintillating crystal that has the highest light output at room and low temperatures among Mo-containing crystals (molybdates) [12, 13].

Choosing of  $^{100}\text{Mo}$  as the source of  $0\nu\beta\beta$  is advantageous. The nucleus has a high  $Q$  value of 3034.40(17) keV [14] that is above the intensive 2615 keV gamma quanta from  $^{208}\text{Tl}$  decay ( $^{232}\text{Th}$  family). The natural abundance of  $^{100}\text{Mo}$  is 9.8% [15], which is comparatively high. Furthermore, enriched  $^{100}\text{Mo}$  can be produced by centrifugation method in amount of tens of kilograms per year with a reasonable price. Also, the theoretically estimated half life of  $^{100}\text{Mo}$  is relatively shorter than that of other  $0\nu\beta\beta$  candidates [16, 17]. However,  $2\nu\beta\beta$  of  $^{48}\text{Ca}$  with  $Q_{\beta\beta} = 4272$  keV (despite rather low concentration of the isotope  $\approx 0.2\%$ ) can be an irremovable background source in the ROI of  $^{100}\text{Mo}$ . The AMoRE collaboration has successfully grown  $^{40}\text{Ca}^{100}\text{MoO}_4$  crystals using  $^{100}\text{Mo}$  enriched and  $^{48}\text{Ca}$  depleted materials. Three of the doubly-enriched crystals with masses in the range of 0.2–0.4 kg were tested in a low background  $4\pi$  veto system to determine their internal backgrounds [18].

The present experimental work aims to test the low temperature detection concept with a  $\text{CaMoO}_4$  crystal and an MMC that is suitable for a high resolution experiment to search for  $0\nu\beta\beta$  of  $^{100}\text{Mo}$ . A 216 g natural  $\text{CaMoO}_4$  crystal with an MMC phonon sensor was employed in this experiment, which was performed in an overground measurement facility. The energy resolution and linearity of the detector setup, particle, and randomly coinciding events discrimination by pulse shape analysis for background rejection in a  $0\nu\beta\beta$  experiment are discussed in this report.

## 2. Experimental Details

The detector setup was structured in a cylindrical shape with copper support details as shown in Figure 1. A  $\text{CaMoO}_4$  crystal, 4 cm in diameter and 4 cm height, was mounted inside the copper structure using metal springs. The mass of the crystal was 216 g. It was grown with natural Ca and Mo elements at the Bogoroditsk plant in Russia. A patterned gold film was evaporated on one side of the crystal to serve as a phonon collector. An MMC device, the primary sensor for detecting the phonon signals absorbed in the gold film, was placed on a semicircular copper plate over the crystal. The thermal connection between the gold film and the MMC was made using annealed gold wires. Details regarding the measurement principle and the detector structure of the MMC device were presented in previous reports [19, 20].

When a particle hits a dielectric material, most of the energy deposited into the absorber is converted into the form of phonons. High energy phonons with frequencies that are close to the Debye frequency are generated initially. However, they quickly decay to lower frequency phonons via anharmonic processes. When their energy becomes 20–50 K, they can travel ballistically in the crystal [21].

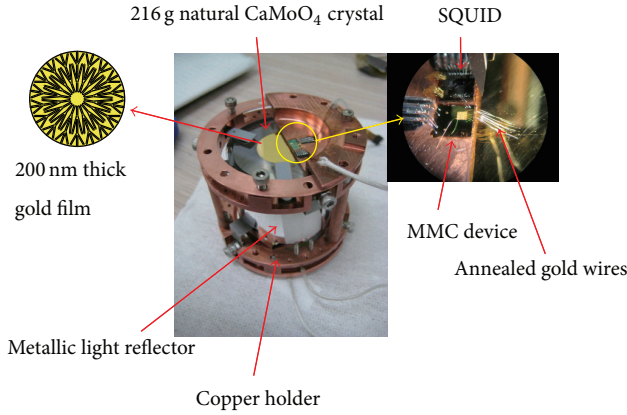


FIGURE 1: (Color online) low temperature detector setup with a 216 g  $\text{CaMoO}_4$  crystal and an MMC sensor.

The major down-conversion processes of these athermal phonons are isotope scattering, inelastic scatterings by impurities and lattice dislocations, and inelastic scatterings at crystal surfaces [22]. These excess phonons eventually change the equilibrium thermal phonon distribution, thereby causing temperature increase.

In the detector setup with the  $\text{CaMoO}_4$  crystal and the gold phonon collector film, the ballistic athermal phonons can hit the crystal and gold interface, transmit into the gold film, and transfer their energy to the electrons in the film [23]. The electron temperature of the gold film increases quickly via electron-electron scatterings. This temperature change is measured by the MMC sensor that is thermally connected with the gold wires. The size of the gold film and number of gold wires were chosen based on a thermal model study that considered the efficient athermal heat flow process [11]. Consequently the gold film had a diameter of 2 cm, a thickness of 200 nm, and an additional gold pattern of 200 nm thickness on top of the gold film to increase the lateral thermal conductivity of the gold film.

The detector assembly was installed in a dilution refrigerator in an underground laboratory at KRISS (Korea Research Institute of Standards and Science). The refrigerator was surrounded by a 10 cm thick lead shield (except the top surface) to reduce environmental gamma-ray background. The detector with an MMC operates well in the temperature range of 10–50 mK. The signal size increases at lower temperatures since the MMC sensitivity enhanced and the heat capacities decreased. However, the signals have slower rise and decay times at lower temperatures as thermal conductances become poorer. Larger signal size improves the energy threshold and baseline energy resolution of the detector. The energy resolution of the detector measured for particle absorption events can be worse than the baseline resolution because of any uncorrelated mechanism that affects the signal size and shape. Examples of such mechanisms include temperature fluctuations due to instrumental instability or frequent event rates, position dependence of signal shapes, or scintillation processes that are associated with phonon generations in an inhomogeneous way. Therefore, larger signal size does not

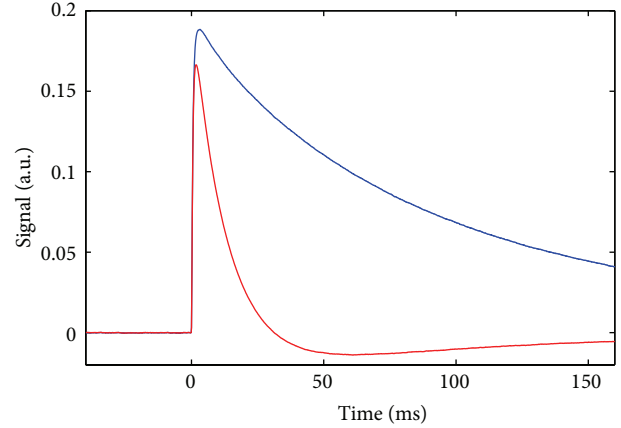


FIGURE 2: (Color online) a typical signal of 2.6 MeV gamma-ray full absorption events at 40 mK in DC (blue, bigger) and AC (red, smaller) coupling.

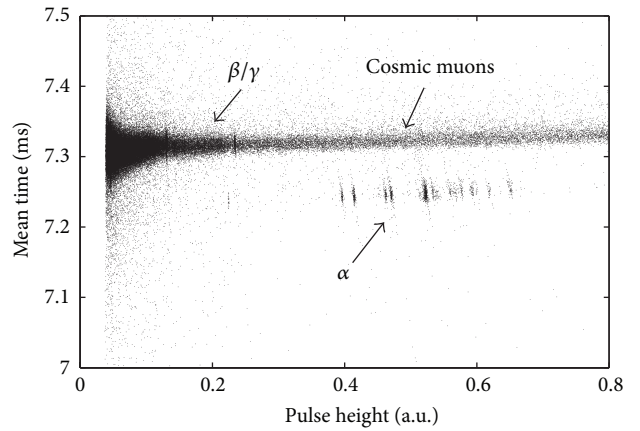


FIGURE 3: A scatter plot of the mean-time and pulse height obtained from the background measurement of 95 h in an underground laboratory.  $\alpha$  and  $\beta/\gamma$  (including cosmic muons) events are clearly separated in terms of their mean-time values.

guarantee a better energy resolution at certain temperatures. At the present experimental condition including the background rate from cosmic muons and external gamma-rays, 40 mK was selected as the main measurement temperature. At this temperature, about 1 ms rise-time was obtained for the 2.6 MeV gamma line without degrading the energy resolution. A typical signal of 2.6 MeV gamma-ray full absorption events is shown in Figure 2. The rise-time of the DC coupled signal is 1.1 ms, which is somewhat slower than that of earlier measurements for which shorter gold wires were used [11].

### 3. Pulse Shape Analysis

A two dimensional scatter plot of the pulse heights and mean-times of signals obtained in a 95 h background measurement is shown in Figure 3. The pulse height is the difference between the maximum value and baseline level of a signal. The maximum value is found using a quadratic polynomial

fit to the region of the signal near the pulse maximum. The baseline level is the average voltage value in the time region before the signal rises. The mean-time parameter is defined as

$$t_{\text{mean}} = \frac{\sum_{t_{10}-l}^{t_{10}+r} (v_t \times (t - t_{10}))}{\sum_{t_{10}-l}^{t_{10}+r} v_t}, \quad (5)$$

where  $v_t$  is the measured voltage value at time  $t$  subtracting the baseline level,  $t_{10}$  is the time when it reaches 10% of the pulse height, and  $l$  and  $r$  indicate the time length of the signal toward left and right directions from  $t_{10}$ , respectively, to calculate the mean-time.  $l$  is set to reach the time at the baseline level, while  $r$  is a free parameter that was selected to achieve the most efficient particle discrimination. Here, the  $r$  value was set to not include the negative part of an AC coupled signal (see Figure 2), which was used for the energy spectrum because it was recorded with finer digitizer resolution (i.e., bigger gain is used) than the DC coupled signal.

The pulse-shape discrimination (PSD) between  $\alpha$  and  $\beta/\gamma$  particles can be realized with the mean-time as a pulse shape parameter due to the difference in the rise and decay times of the two types of events. A similar tendency of PSD was reported for other low temperature scintillating detectors [24]. The separation into two groups of the events in the energy region between 4 and 5 MeV of alpha-equivalent energy can be readily observed from the distribution of mean-time values shown in Figure 4. The energy of  $\alpha$  induced events was determined as described in the following section. Although the two peaks have noticeable right-hand tails toward higher mean-time values, normal Gaussian functions were used to fit the distributions. We interpret the right-hand tails as a result of signal pile-up. A parameter of discrimination power (DP) is defined as

$$DP = \frac{\mu_1 - \mu_2}{\sqrt{\sigma_1^2 + \sigma_2^2}}, \quad (6)$$

where  $\mu_i$  are the mean values and  $\sigma_i$  are the standard deviations of the Gaussian distributions for  $\alpha$  and  $\beta/\gamma$  events. DP was found to be 7.6.

The averaged pulse shapes for the two groups of events are compared in Figure 5. Templates of  $\alpha$  events were obtained by averaging out the  $^{232}\text{Th}$   $\alpha$ -decay events pulse profiles with energy release in the crystal 4082 keV (due to the contamination of the crystal by thorium), whereas the events caused by cosmic muons with the same pulse height were selected for the template of  $\beta$  induced events. The normalized pulses of alpha and beta templates are aligned at the time of their maximum values, as shown in Figure 5. Both the rise and decay times of the  $\alpha$  and  $\beta$  signals are clearly different. The signals induced by  $\alpha$  events have faster rise and faster decay than those of the  $\beta$  events.

According to scintillation measurements of a  $\text{CaMoO}_4$  crystal at 7–300 K [25, 26], the scintillation decay time of the  $\text{CaMoO}_4$  crystal reaches hundreds of  $\mu\text{s}$  at 7 K. The crystal also shows different light outputs for  $\alpha$  and  $\beta/\gamma$

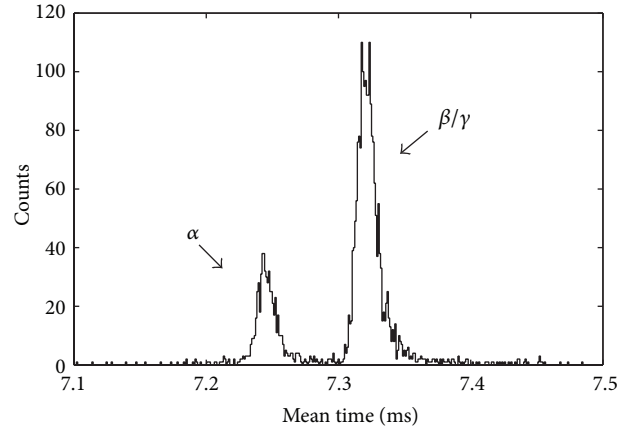


FIGURE 4: Distribution of mean-time parameter in  $4 \text{ MeV} < E < 5 \text{ MeV}$  region of alpha-equivalent energy. Discrimination power was found to be 7.6 from fitting each group of distribution with a normal Gaussian function. Right-hand side tail is noticeable for the two groups toward higher mean-time value.

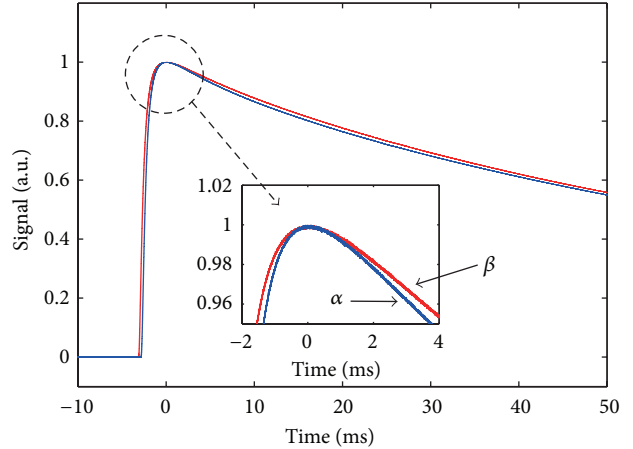


FIGURE 5: (Color online) averaged pulse shapes of  $\alpha$  induced signals from  $^{232}\text{Th}$  decays (blue) and the corresponding (i.e., with the same pulse height) muon-induced signals (red). The signals are normalized for their pulse height and shifted in time to align the maximum point of signals.

events [27]. A slowly decaying scintillation mechanism would cause slow generation of phonon in the  $\text{CaMoO}_4$  crystal.  $\alpha$  and  $\beta/\gamma$  particle events may have different fractions of slow component for phonon generation. This difference in slow phonon generation at mK temperatures may induce different pulse shapes for  $\alpha$  and  $\beta/\gamma$  particle events.

## 4. Energy Spectrum

Because athermal phonon absorption in the phonon collector significantly contributes to the signal size [11], the signals have some degrees of position dependence for their pulse height and shape. In this detector, the signals with faster rise-times show bigger pulse heights for the same energy events. This effect can be observed in Figure 3. The distribution of

mean-time values and pulse heights for alpha and gamma-ray full absorption lines has anticorrelated slopes. This negative slope more dominantly appears in the alpha signals, which is likely because the full-energy  $\gamma$  peaks originate from multiple Compton scatterings in the crystal that smear the position dependence on the event location. The pulse height is not an optimal parameter to obtain a high resolution. In the optimal filtering method [28] that is often adopted in high resolution microcalorimeters, the signals are assumed to have one shape but with different amplitudes. Thus, the optimal filtering method is not applicable to provide a high resolution spectrum for the present signals.

In the present analysis, a new parameter LA (left area) was used as an amplitude parameter to reduce the position dependence effect of the large crystal detector. It is defined as

$$LA = \sum_{t_{10}-l}^{t_{\text{mean}}} v_t, \quad (7)$$

where the variables are as defined in (5). LA is a partial integration for the leading part of a signal. Because the integration range of the LA parameter is set by a shape-dependent parameter, the mean-time, this parameter is less influenced by the pulse shape. For instance, the correlation coefficient between the pulse height and mean-time was  $-0.62$  for  $4082$  keV  $\alpha$  signals, but it was  $0.08$  between the LA and mean-time.

In a calibration run, a thoriated tungsten rod was used as an external gamma-ray source. The source was placed in the gap between the cryostat and the lead shield.

When a linear energy calibration was applied to gamma-ray peaks, deviations from the linear calibration of less than  $0.4\%$  were found for low-energy peaks. A quadratic function with no constant term was used for the calibration of electron-equivalent energy for  $511$ ,  $583$ ,  $911$ , and  $2615$  keV peaks for the spectrum shown in Figure 6. The corresponding energy resolutions of the peaks are listed in Table 1.

Figure 7 shows the linearities of the electron and alpha signals. The LA values of the electron and alpha peaks divided by the linear calibration of the gamma-ray peaks are plotted in the upper figure. The LA/energy ratios for the alpha peaks are about  $6\%$  larger than those for the gamma-ray peaks. The quadratic fit functions are shown as dotted and dashed lines for gamma and alpha peaks, respectively. The residuals in the lower figure indicate deviations from the quadratic functions for the two groups. With the quadratic calibration, a very small deviation is expected near  $3$  MeV for electron measurements. It implies that this method can supply an accurate energy calibration at the  $Q_{\beta\beta}$  value of the  $2\nu\beta\beta$  of  $^{100}\text{Mo}$ .

Alpha events can be separated from  $\beta/\gamma$  events using the mean-time parameter. The energy spectrum of alpha events is shown in Figure 8. An energy calibration for this spectrum was performed with a quadratic function for the alpha peaks as discussed above. These backgrounds were bulk events of alpha decays in the crystal, mainly from radionuclides of U and Th decay chains, most of them are identified as shown in Figure 8. Because this crystal was developed to investigate the scintillation properties of  $\text{CaMoO}_4$ , its internal

TABLE 1: Energy resolutions of gamma-ray full absorption peaks in the calibration measurement.

Energy (keV)	FWHM (keV)
511	$7.2 \pm 0.6$
583	$6.5 \pm 0.5$
911	$6.8 \pm 0.3$
2615	$10.9 \pm 0.4$

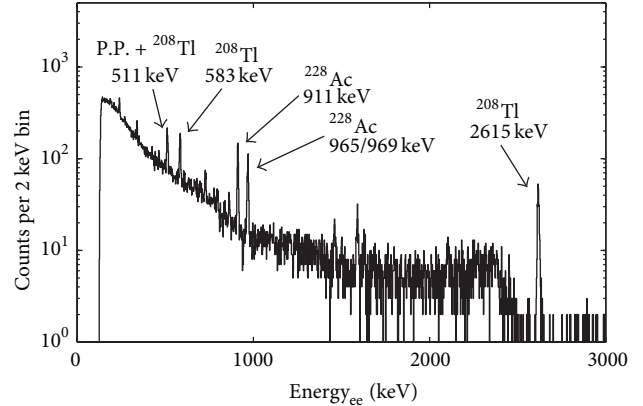


FIGURE 6: Energy spectrum measured with an external source over 65 h.

background was not exceptionally low. The AMoRE collaboration has developed  $^{40}\text{Ca}^{100}\text{MoO}_4$  growing technology with low radioimpurities. Internal alpha activities of about  $80 \mu\text{Bq/kg}$  of  $^{226}\text{Ra}$  and  $70 \mu\text{Bq/kg}$  of  $^{228}\text{Th}$  were found in a  $196 \text{ g } ^{40}\text{Ca}^{100}\text{MoO}_4$  [18].

Not only alpha signals can be rejected efficiently, but also  $\beta$  decays of  $^{212}\text{Bi}$ ,  $^{214}\text{Bi}$ , and  $^{208}\text{Tl}$  can be tagged and eliminated from the data by using information about associated alpha-emitting nuclides. Random pile-ups of events (first of all from the  $2\nu\beta\beta$ ) could be a substantial source of background of LTD to search for  $0\nu\beta\beta$  due to the poor time resolution [29]. Relatively fast response of the MMC among the LTDs is a certain advantage to discriminate the background.

## 5. Conclusion

LTDs made of crystal scintillators containing isotopes of interest have distinct advantages in  $0\nu\beta\beta$  searches. Such LTDs make it possible to provide a high detection efficiency to the  $0\nu\beta\beta$ . Taking the advantage of high resolution sensor technologies, these dielectric detectors in the heat (phonon) measurement can have comparable energy resolution to those of HPGe detectors. The comparison in heat/light measurement channels makes unambiguous separation of alpha events from electron events. As discussed in this report, pulse shape discrimination is also possible using only the phonon measurement. This PSD capability of the phonon sensor increases discrimination power for alpha background signals or can simplify the detector cell design by using only one phonon sensor without a photon sensor that is commonly

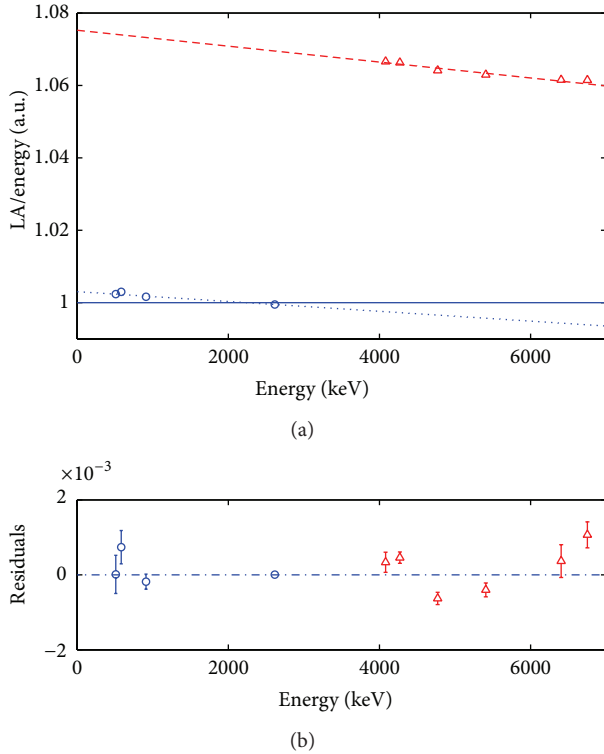


FIGURE 7: (Color online) ratio of signal amplitude (LA) and energy in linear calibration for  $\gamma$  (circle, blue) and  $\alpha$  (triangle, red) peaks (a). Quadratic calibration lines (dotted and dashed lines) are shown for  $\gamma$  and  $\alpha$  peaks, respectively. Deviations of the ratios from each quadratic functions are shown in (b).

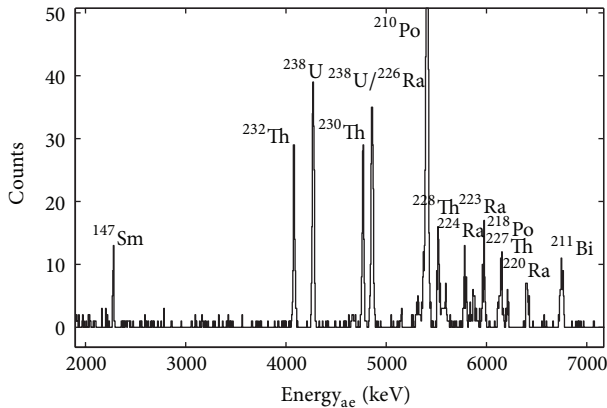


FIGURE 8: Energy spectrum of bulk alpha events in a background measurement.

used for particle discrimination [30] and will reduce the number of measurement channels.

In comparison with signals from PMTs or conventional semiconductor detectors, phonon signals from a crystal detector in the LTD concept are typically slow. Even though the energy resolution of these detectors does not suffer from the slow signal in the low activity environment of an underground experiment, random coincidence of events

leads to an unavoidable background because of the slow rise-time [29]. Two consecutive electron events that occur in a time interval that is much shorter than the signal rise-time can be regarded as a single event. Such randomly coincident events, particularly of  $2\nu\beta\beta$ , are an unavoidable source of backgrounds in the  $0\nu\beta\beta$  taking into account that the  $2\nu\beta\beta$  event rate of  $^{100}\text{Mo}$  is expected to be about 10 mBq in 1 kg  $^{40}\text{Ca}^{100}\text{MoO}_4$ .

In the present experiment, the phonon signals had rise-times of 1.1 ms, which is much faster than the rise-times of LTDs with NTD Ge thermistors. The fast rise-time provides efficient rejection possibility for randomly coincident events [31]. Moreover, a photon detector composed of a 2 inch Ge wafer and an MMC sensor showed a temperature independent rise-time of about 0.2 ms with reasonable energy resolution [32]. Simultaneous measurements with the photon detector will increase the discrimination power not just for alpha events but also for randomly coincident events.

For the AMoRE project,  $^{40}\text{Ca}^{100}\text{MoO}_4$  crystals will be used as the detector material together with MMCs in phonon and photon measurement setups. We aim to reach a zero background with improved energy resolution of a few keV. The first stage experiment is expected to be constructed with a 10 kg prototype detector by 2016. We plan to perform a large scale experiment with 200 kg  $^{40}\text{Ca}^{100}\text{MoO}_4$  crystals in the next 5-6 years. The sensitivity of the experiment to the effective Majorana neutrino mass is estimated to be in the range of 20–50 meV, which corresponds to the inverted scheme of the neutrino mass.

## Conflict of Interests

The authors declare that there is no conflict of interests regarding the publication of this paper.

## Acknowledgments

This research was funded by Grant no. IBS-R016-G1 and partly supported by the National Research Foundation of Korea Grant funded by the Korean Government (NRF-2011-220-C00006 and NRF-2013K2A5A3000039). F. A. Danevich was supported in part by the Space Research Program of the National Academy of Sciences of Ukraine.

## References

- [1] J. Beringer, J. F. Arguin, R. M. Barnett et al., “Review of particle physics,” *Physical Review D*, vol. 86, Article ID 010001, 2012.
- [2] R. N. Mohapatra, S. Antusch, K. S. Babu et al., “Theory of neutrinos: a white paper,” *Reports on Progress in Physics*, vol. 70, no. 11, pp. 1757–1867, 2007.
- [3] S. R. Elliott and P. Vogel, “Double beta decay,” *Annual Review of Nuclear and Particle Science*, vol. 52, pp. 115–151, 2002.
- [4] F. T. Avignone, S. R. Elliott, and J. Engel, “Double beta decay, Majorana neutrinos, and neutrino mass,” *Reviews of Modern Physics*, vol. 80, p. 481, 2008.
- [5] W. Rodejohann, “Neutrino-less double beta decay and particle physics,” *International Journal of Modern Physics E*, vol. 20, no. 9, pp. 1833–1930, 2011.

- [6] A. Giuliani and A. Poves, “Neutrinoless double-beta decay,” *Advances in High Energy Physics*, vol. 2012, Article ID 857016, 38 pages, 2012.
- [7] J. J. Gómez-Cadenas, J. Martín-Albo, M. Mezzetto, F. Monrabal, and M. Sorel, “The search for neutrinoless double beta decay,” *Rivista del Nuovo Cimento*, vol. 35, no. 2, pp. 29–98, 2012.
- [8] C. Enss, *Cryogenic Particle Detection*, vol. 99, Springer, 2005.
- [9] H. Bhang, R. S. Boiko, D. M. Chernyak et al., “AMoRE experiment: a search for neutrinoless double beta decay of  $^{100}\text{Mo}$  isotope with  $^{40}\text{Ca}^{100}\text{MoO}_4$  cryogenic scintillation detector,” *Journal of Physics: Conference Series*, vol. 375, no. 4, Article ID 042023, 2012.
- [10] S. J. Lee, J. H. Choi, F. A. Danevich et al., “The development of a cryogenic detector with  $\text{CaMoO}_4$  crystals for neutrinoless double beta decay search,” *Astroparticle Physics*, vol. 34, no. 9, pp. 732–737, 2011.
- [11] G. B. Kim, S. Choi, Y. S. Jang et al., “Thermal model and optimization of a large crystal detector using a metallic magnetic calorimeter,” *Journal of Low Temperature Physics*, vol. 176, no. 5–6, pp. 637–643, 2014.
- [12] H. J. Kim, A. N. Annenkov, R. S. Boiko et al., “Neutrino-less double beta decay experiment using  $\text{Ca}_{100}\text{MoO}_4$  scintillation crystals,” *IEEE Transactions on Nuclear Science*, vol. 57, no. 3, pp. 1475–1480, 2010.
- [13] S. Pirro, J. W. Beeman, S. Capelli, M. Pavan, E. Previtali, and P. Gorla, “Scintillating double-beta-decay bolometers,” *Physics of Atomic Nuclei*, vol. 69, no. 12, pp. 2109–2116, 2006.
- [14] S. Rahaman, V.-V. Elomaa, T. Eronen et al., “Q values of the  $^{76}\text{Ge}$  and  $^{100}\text{Mo}$  double-beta decays,” *Physics Letters B: Nuclear, Elementary Particle and High-Energy Physics*, vol. 662, no. 2, pp. 111–116, 2008.
- [15] M. E. Wieser and J. R. D. Laeter, “Absolute isotopic composition of molybdenum and the solar abundances of the  $p$ -process nuclides  $^{92,94}\text{Mo}$ ,” *Physical Review C*, vol. 75, Article ID 055802, 2007.
- [16] J. Barea, J. Kotila, and F. Iachello, “Limits on neutrino masses from neutrinoless double- $\beta$  decay,” *Physical Review Letters*, vol. 109, no. 4, Article ID 042501, 2012.
- [17] J. D. Vergados, H. Ejiri, and F. Šimkovic, “Theory of neutrinoless double-beta decay,” *Reports on Progress in Physics*, vol. 75, no. 10, Article ID 106301, 2012.
- [18] J. H. So, H. J. Kim, V. V. Alenkov et al., “Scintillation properties and internal background study of  $^{40}\text{Ca}^{100}\text{MoO}_4$  crystal scintillators for neutrino-less double beta decay search,” *IEEE Transactions on Nuclear Science*, vol. 59, no. 5, pp. 2214–2218, 2012.
- [19] W. S. Yoon, Y. S. Jang, G. B. Kim et al., “High energy resolution cryogenic alpha spectrometers using magnetic calorimeters,” *Journal of Low Temperature Physics*, vol. 167, no. 3–4, pp. 280–285, 2012.
- [20] W. S. Yoon, G. B. Kim, H. J. Lee et al., “Fabrication of metallic magnetic calorimeter for radionuclide analysis,” *Journal of Low Temperature Physics*, vol. 176, no. 5–6, pp. 644–649, 2014.
- [21] J. P. Wolfe, *Imaging Phonons: Acoustic Wave Propagation in Solids*, Cambridge University Press, 2005.
- [22] S. W. Leman, “Invited review article: physics and Monte Carlo techniques as relevant to cryogenic, phonon, and ionization readout of Cryogenic Dark Matter Search radiation detectors,” *Review of Scientific Instruments*, vol. 83, Article ID 091101, 2012.
- [23] Y. H. Kim, H. Eguchi, C. Enss et al., “Measurements and modeling of the thermal properties of a calorimeter having a sapphire absorber,” *Nuclear Instruments and Methods in Physics Research A: Accelerators, Spectrometers, Detectors and Associated Equipment*, vol. 520, no. 1–3, pp. 208–211, 2004.
- [24] C. Arnaboldi, C. Brofferio, O. Cremonesi et al., “A novel technique of particle identification with bolometric detectors,” *Astroparticle Physics*, vol. 34, no. 11, pp. 797–804, 2011.
- [25] V. B. Mikhailik, S. Henry, H. Kraus, and I. Solskii, “Temperature dependence of  $\text{CaMoO}_4$  scintillation properties,” *Nuclear Instruments and Methods in Physics Research A*, vol. 583, no. 2–3, pp. 350–355, 2007.
- [26] V. B. Mikhailik and H. Kraus, “Performance of scintillation materials at cryogenic temperatures,” *Physica Status Solidi B*, vol. 247, no. 7, pp. 1583–1599, 2010.
- [27] A. N. Annenkov, O. A. Buzanov, F. A. Danevich et al., “Development of  $\text{CaMoO}_4$  crystal scintillators for a double beta decay experiment with  $^{100}\text{Mo}$ ,” *Nuclear Instruments and Methods in Physics Research A*, vol. 584, no. 2–3, pp. 334–345, 2008.
- [28] Y. N. Yuryev, Y. S. Jang, S. K. Kim et al., “Signal processing in cryogenic particle detection,” *Nuclear Instruments and Methods in Physics Research A: Accelerators, Spectrometers, Detectors and Associated Equipment*, vol. 635, no. 1, pp. 82–85, 2011.
- [29] D. M. Chernyak, F. A. Danevich, A. Giuliani, E. Olivieri, M. Tenconi, and V. I. Tretyak, “Random coincidence of  $2\nu2\beta$  decay events as a background source in bolometric  $0\nu2\beta$  decay experiments,” *European Physical Journal C*, vol. 72, no. 4, pp. 1–6, 2012.
- [30] D. Artusa, F. Avignone III, O. Azzolini et al., “Exploring the neutrinoless double beta decay in the inverted neutrino hierarchy with bolometric detectors,” <http://arxiv.org/abs/1404.4469>.
- [31] D. M. Chernyak, F. A. Danevich, A. Giuliani et al., “Rejection of randomly coinciding events in  $\text{ZnMoO}_4$  TeX scintillating bolometers,” *The European Physical Journal C*, vol. 74, p. 2913, 2014.
- [32] H. J. Lee, C. S. Kang, S. R. Kim et al., “Development of a scintillation light detector for a cryogenic rare-event-search experiment,” submitted in *Nuclear Instruments and Methods in Physics Research Section A*.



**Hindawi**

Submit your manuscripts at  
<http://www.hindawi.com>

